arXiv:cond-mat/0205465v1 [cond-mat.dis-nn] 23 May 2002

Bistable Gradient Networks II: Storage Capacity and Behaviour Near Saturation

Patrick McGraw and Michael Menzinger

University of Toronto
(Dated: December 27, 2021)

We examine numerically the storage capacity and the behaviour near saturation of an attractor neural network consisting of bistable elements with an adjustable coupling strength, the Bistable Gradient Network (BGN). For strong coupling, we find evidence of a first-order "memory blackout" phase transition as in the Hopfield network. For weak coupling, on the other hand, there is no evidence of such a transition and memorized patterns can be stable even at high levels of loading. The enhanced storage capacity comes, however, at the cost of imperfect retrieval of the patterns from corrupted versions.

PACS numbers: 07.05.Mh,42.65.Pc,42.79.Ta,42.82.Ds,84.35.+i,87.18

I. INTRODUCTION

In this paper we consider the behaviour at high memory loading of a Hopfield-like attractor network of N bistable elements, the bistable gradient network or BGN[1][12]. This is a sequel to an earlier paper [2] which considered the BGN at low loading. We compare the BGN to the deterministic Hopfield network (HN)[3]-[9], examining the storage capacity and other key properties.

To begin, we review the BGN model and establish some notation. The BGN is described by the coupled differential equations

$$\frac{dx_i}{dt} = -\frac{\partial H}{\partial x_i}, \tag{1}$$

where x_i are N continuous-valued real variables (or components of an N-dimensional state vector $\mathbf{x}$) representing the outputs of the N nodes of the network, and H is the Hamiltonian

$$H = H_0 + H_{int} = \sum_{i=1}^{N}\left(\frac{x_i^4}{4} - \frac{x_i^2}{2}\right) - \frac{1}{2}\gamma\sum_{i,j=1}^{N} w_{ij}x_i x_j. \tag{2}$$

The quantities w_{ij} are the elements of a symmetric matrix of connection strengths and γ is a control parameter determining the overall strength of the coupling among nodes. As in the Hopfield model[3][4], the connections or synaptic weights are determined by the Hebb learning rule[10]

$$w_{ij} = \frac{1}{N}\sum_{\mu=1}^{p}\xi_i^\mu\xi_j^\mu - \frac{p}{N}\delta_{ij} \tag{3}$$

where the N-dimensional vectors $\boldsymbol{\xi}^\mu$ represent a set of p distinct *memory patterns* to be recognized by the network. We take these patterns to consist of binary elements ± 1 only, and we assign them random values, thus introducing quenched disorder. The BGN's key difference from the HN and from most of its continuous-valued relatives [11] lies in the presence of the local quartic potential term H_0 in the Hamiltonian, which renders each node bistable.

The interaction term H_{int} furnishes an input to each node given by $h_i = \gamma\sum_{\mu=1}^{p} w_{ij}x_j$ so that the dynamical equation for each node is given by

$$\frac{dx_i}{dt} = x_i - x_i^3 + h_i. \tag{4}$$

The input may also be referred to as a "magnetic field" by analogy with Ising spin systems. In the absence of input each node has two stable fixed points at ± 1, but a nonzero field shifts the two fixed points. If the critical magnitude $h_c = \frac{2\sqrt{3}}{9} \approx 0.38$ is exceeded then the field is strong enough to overcome the potential barrier in the quartic potential and there is then only one fixed point.

We define two sets of order parameters m_μ and b_μ by

$$m_\mu \equiv \boldsymbol{\xi}^\mu \cdot \mathbf{x} = \frac{1}{N}\sum_{i=0}^{N}\xi_i^\mu x_i \tag{5}$$

and

$$b_\mu \equiv \frac{1}{N}\sum_{i=0}^{N} \xi_i^\mu \,\mathrm{sign}(x_i). \tag{6}$$

m_μ are inner products or overlaps of the state vector with the memorized patterns, while b_μ, the "bit overlaps," encode information about sign agreements between the state vector and the stored patterns. For the purposes of this paper, we will for the most part be more interested in b_μ than in m_μ, so where there is little risk of confusion we will drop the word "bit" and simply refer to b_μ as an "overlap."

The degree of loading of the network's memory can be parametrized by the ratio $\alpha \equiv p/N$. In the companion paper [2] we examined the behaviour of the BGN in the low-loading limit $\alpha \ll 1$. It was shown that the network can function as an associative memory and correct sign flip errors in a stored pattern as long as $\gamma > \frac{1}{3}$. We found that the attractors of the BGN's dynamics are readily classified into three categories which are separated from each other in energy. The lowest energy states are the *memory* or *retrieval states*, each of which corresponds to one of the memorized patterns. In addition to these there are higher-energy spurious attractors of two types. The *mixture* or *spin glass states* have partial overlaps with several patterns and thus lie close to the subspace spanned by the memory patterns. *Uncondensed states*, which have no counterpart in the HN, are states in which none of the fields acting on the nodes are strong enough to cause sign flips and the dynamics is therefore dominated by the local potential. They have energies per node close to -0.25. The spin glass states are intermediate in energy between the memory states and the uncondensed states. In the range $\frac{1}{3} \leq \gamma \lessapprox 1$, pattern recognition by the network was found to be highly selective; the input must be close to the stored pattern in order for the pattern to be fully restored. The uncondensed states are numerous (of order 2^N) and fill most of the configuration space. The memorized patterns and their basins of attraction occupy isolated valleys among these states, but these valleys expand as γ increases. For $\gamma \gtrapprox 1$, on the other hand, the behaviour resembles that of the HN: there are no uncondensed states, and the memory states have large basins of attraction.

In this paper we turn to the case where p/N is of order unity. We are interested in the maximum storage capacity, or the maximum number of patterns that can be successfully stored and retrieved, as well as changes in the network's performance as this limit is approached. Earlier work with small networks [12] suggested that at least under certain conditions the BGN could store many more patterns than the HN while possessing few spurious attractors. It is known that the Hopfield storage limit of $p \approx 0.14N$ memory patterns can be exceeded if a more complicated learning algorithm is used [9], but in the BGN case improved capacity is achieved with the familiar Hebb rule. Since the previous results [1][12] were obtained with networks much too small to be of practical interest (e.g., $N = 5$), we now examine larger networks, mainly through numerical simulations. (At the end of the paper we will return briefly to the small-network case.) We find that the high-loading behaviour, like that at low loading, depends strongly on γ. For $\gamma \gtrsim 1$, a Hopfield-like first-order phase transition results in the destabilization of all memory states at a critical value of α. For $\gamma = 2$ this transition occurs at $\alpha_c \approx 0.1$, compared to $\alpha_c \approx 0.14$ for the HN. For $\gamma = 0.5$, on the other hand, we find that it is possible for the stored patterns to remain stable even at loading factors of $\alpha \approx 0.3$ and higher. Furthermore, there is no sudden blackout; instead, the performance degrades gradually as α increases. The price of this high capacity is that the retrieval of the patterns from corrupted versions may be imperfect.

The remainder of the paper is organized as follows: In section II we discuss in general terms the effects of crosstalk, or interference between different stored patterns. It is crosstalk which is responsible for limitations on storage capacity. We compare the effects of crosstalk in the BGN and the HN. This discussion provides a framework for interpreting our numerical results. In section III we examine numerically the stability of memory patterns as a function of α. We find evidence of a first-order memory blackout phase transition in the BGN at high γ, but not at low γ. In section IV, we examine the effects of high loading on the basins of attraction for the memory states and on their retrieval from corrupted input. We see that increasing the loading markedly alters the energy landscape. In section V we comment briefly on the behaviour of smaller networks and on the relation between the previous small network results [1][12] and those we have obtained for larger networks. We conclude with some discussion of the BGN results and possible directions for further study. We make some conjectures concerning the performance of the BGN in the presence of stochastic noise.

II. PATTERN RETRIEVAL AND CROSSTALK

In a given state $\mathbf{x}$, the input to the i-th node of the network can be expressed as

$$h_i = \gamma \sum_{j=1}^{N} w_{ij} x_j = \gamma \sum_{\mu=1}^{p} \xi_i^\mu m_\mu - \gamma \frac{p}{N} x_i, \tag{7}$$

using the Hebb rule (3) and the definition (5) of m_μ. In [2], we showed that when $\alpha \ll 1$ there are stable retrieval states in which $b_\nu = 1$ for one particular ν. For a state in which the ν-th overlap is large, we can decompose the field as follows:

$$\begin{aligned} h_i &= \gamma \left(\xi_i^\nu m_\nu + \sum_{\mu \neq \nu} \xi_i^\mu m^\mu - \frac{p}{N} x_i \right) \\ &= \gamma \left(S_i + C_i - \frac{p}{N} x_i \right). \end{aligned} \tag{8}$$

We refer to the first term, S_i, as the "signal" term and the second term, C_i, as the "crosstalk" term. In the limit $\frac{p}{N} \to 0$, the mutual overlaps between different patterns is small, so that $m_\nu \ll 1$ ($\nu \neq \mu$), and the last two terms in (8) can be neglected. The signal term is then dominant and there is a stable retrieval state given by $\mathbf{x} = \sqrt{1+\gamma}\boldsymbol{\xi}^\nu$ with $m_\nu = \sqrt{1+\gamma}$. We expect this solution to be approximately valid for small but nonzero values of $\frac{p}{N}$. For this case, the overlaps m_μ ($\mu \neq \nu$) behave as Gaussian distributed random variables with zero mean and variance $1/\sqrt{N}$. Accordingly, the crosstalk term $C_i \equiv \sum_{\mu \neq \nu} \xi_i^\mu m^\mu$ in (8), being a sum of p such quantities, is a random quantity with zero mean and variance $\sqrt{p/N}$. The third term, which arises from the subtraction of the diagonal elements, is of order p/N and thus is generally smaller than the crosstalk term. We will neglect it for the moment.

In the absence of crosstalk, a retrieval state is not only linearly stable (i.e., stable against small perturbations) but, for $\gamma > \frac{1}{3}$, it is also stable against individual sign flips. The latter means that if a retrieval state is corrupted by changing the sign of one or a small number $\ll N$ of nodes, then the dynamics will reverse the flipped sign and restore the pattern. This happens because, in the absence of crosstalk, each node experiences a field $\gamma S_i = \gamma \xi_i^\nu m_\nu$ which has the same sign as ξ_i^ν and for $\gamma > \frac{1}{3}$ that field is strong enough to overcome the potential barrier of the individual node. Now consider a given node (say, the i-th node) in the presence of crosstalk. The crosstalk field acting on the i-th node may be either aligned with or opposed to x_i. If it is aligned, then its effect on that node is to increase the magnitude of x_i, making it larger than $\sqrt{1+\gamma}$. If it is opposed to x_i, then its effect is to *decrease* the equilibrium magnitude of x_i. If the crosstalk term is large enough, then it may be sufficient to overcome the local potential barrier and reverse the sign of x_i, thus introducing a sign error into the pattern. This will occur only if

$$C_i + S_i < -\frac{2\sqrt{3}}{9\gamma}.$$

By contrast, in the Hopfield model a sign error is introduced if

$$C_i + S_i < 0.$$

Thus the relative strength of crosstalk required to introduce sign errors is greater for the BGN than for the HN, and the discrepancy is greatest for small values of γ. One might expect that this would make the BGN less vulnerable to crosstalk (and the memory states more stable) than the HN, especially at low γ, but this is not a foregone conclusion as the BGN's dynamics include mechanisms which tend to amplify small initial overlaps[2] and could conceivably also amplify crosstalk. Our numerical results confirm that the BGN is in fact less prone to crosstalk-induced errors at low values of γ, but not at high values.

If

$$-\frac{2\sqrt{3}}{9\gamma} < C_i + S_i < \frac{2\sqrt{3}}{9\gamma}$$

the crosstalk will not be strong enough to reverse the sign of x_i if initially x_i is correctly aligned with ξ_i^ν, but it will nonetheless destroy the stability against a sign flip. In other words, if x_i is initially misaligned, it will not be corrected. We may say that the node is *"bistabilized"* but not destabilized. (Such an effect cannot occur in the HN where the nodes are not individually bistable.) Since the crosstalk is random, it will in general bistabilize some nodes and not others, with the result that the memory state will be stable against sign flips of certain nodes but not of others. Thus, even though a memory state may be linearly stable, the dynamics may only be able to correct some sign errors, not all. This contrasts with the low-loading case where crosstalk is negligible and there is a single threshold coupling strength, $\gamma = \frac{1}{3}$, above which any single sign error can be corrected. In general, crosstalk results in non-uniform behaviour among nodes, including different magnitudes of x_i for different i.

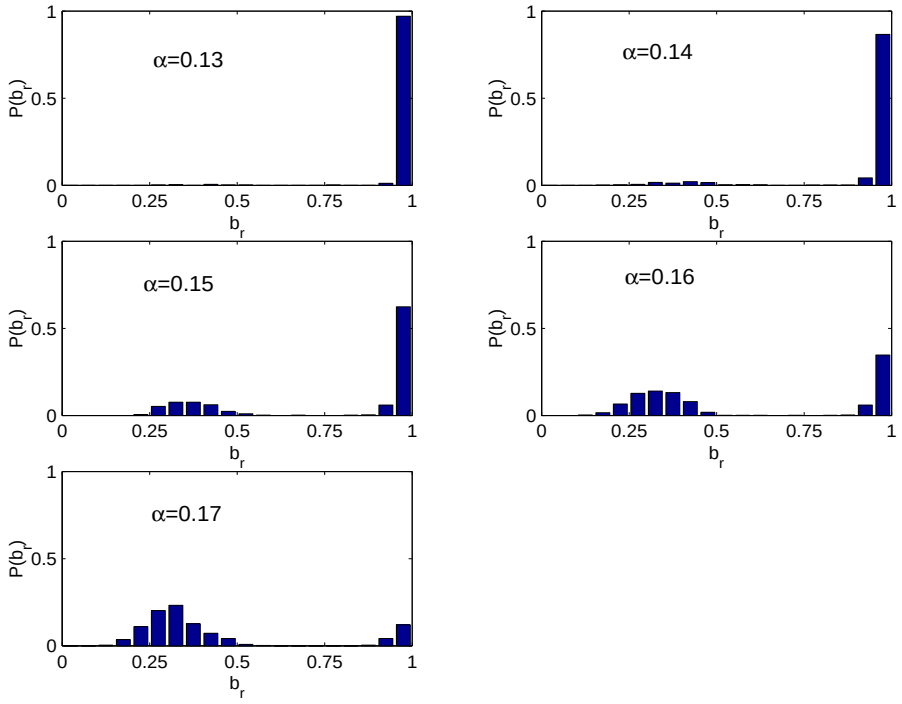


FIG. 1: A series of remanent overlap histograms for a HN with N=2000 nodes, at different values of the loading fraction $\alpha \equiv p/N$. When the critical loading $\alpha_c \cong 0.148$ is exceeded, the strong peak at $b_r > 0.95$ decays and another peak appears at. $b_r \approx 0.3$

III. STABILITY OF THE MEMORY STATES AND REMANENT OVERLAP

To examine the stability of the memory states, we followed a procedure similar to that of reference [9]. Using an ensemble of realizations of the random patterns, we made a number of trials in which the network was initialized to the state $\mathbf{x} = \boldsymbol{\xi}^{\nu}$ for some pattern ν. The initial bit overlap b_ν was thus equal to 1. We then allowed the state to evolve until an attractor was reached. In each case we measured the final energy as well as the bit overlap between the initial and final states, to which we refer as the *remanent* bit overlap b_r. We then constructed histograms showing the probabilities $P(b_r)$ for b_r falling in intervals of width 0.05. Each of the histograms discussed in this section represents an ensemble of at least 200 initial conditions. If the memory state is entirely stable, as is the case at very low loading, then after the dynamics converges the final bit overlap will still be equal to 1. For higher loading, however, the crosstalk fields may introduce sign errors so that $b_r < 1$.

A. HN and BGN with high γ

First consider the case of the HN. Figure 1 shows a series of $P(b_r)$ histograms for the HN at different values of $\alpha = p/N$. (The data here are our own, but the results are comparable to those given in [9]. We include them for comparison with BGN results.) At lower levels of loading, crosstalk introduces few errors, so $b_r > 0.95$ in the large majority of cases. However, as α increases beyond the critical value $\alpha_c \approx 0.148$, the high-b_r peak of the distribution begins to vanish and a second, broader peak begins to grow in the vicinity of $b_r \approx 0.3$. The states in the second peak are spin glass states. As shown in figure 2, this transition becomes sharper with increasing network size, and finite-size scaling analysis shows behaviour characteristic of a first order phase transition in the thermodynamic limit [9]. In the limit $N \to \infty$ the associative memory fails suddenly as the critical loading is exceeded— the remanent overlap drops abruptly from near 1 to 0.3. This nonzero value of the remanent overlap above the critical loading was noted in [9] and attributed to replica symmetry breaking, as the replica symmetric theory predicts that b_r should drop to zero above the phase transition. This phenomenon is related to the non-zero remanent magnetization of a spin glass [13].

In the BGN with $\gamma = 2$, a similar transition evidently occurs at $\alpha_c \approx 0.1$. As evidence, in figure 3 we show two

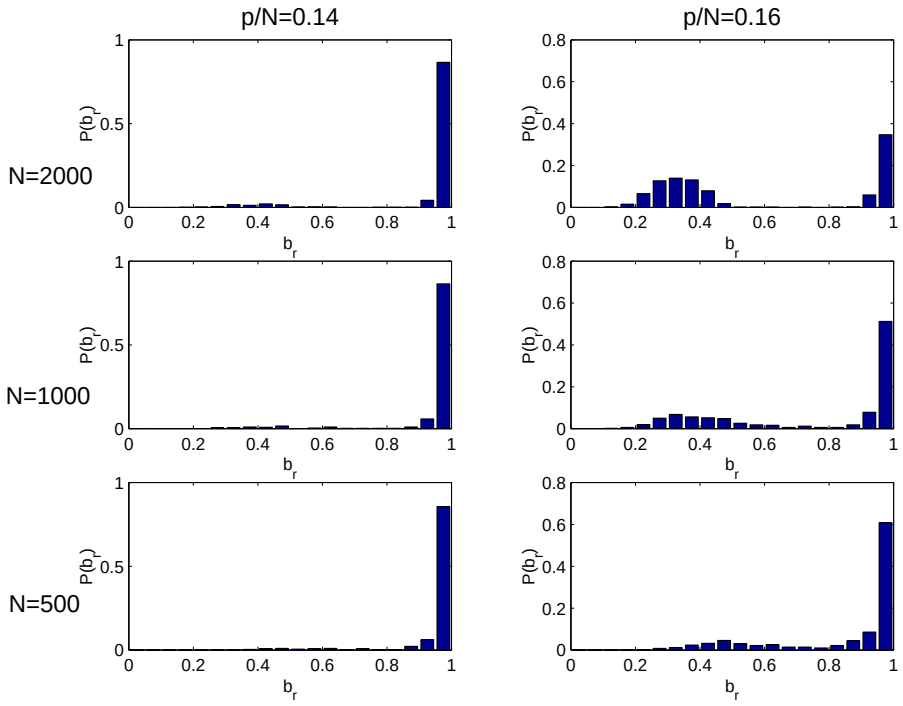


FIG. 2: Remanent overlap histograms for the Hopfield network below the critical loading (left column) and above (right column), showing finite size effects. The transition becomes sharper as N increases.

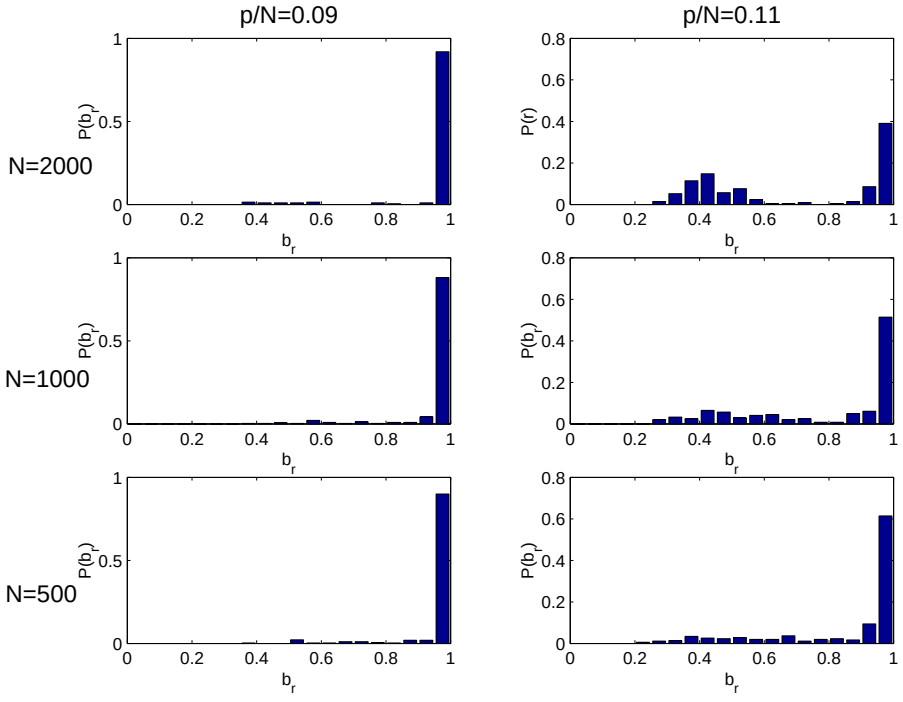


FIG. 3: Remanent overlap histograms for the BGN with $\gamma = 2$ show evidence of a first-order transition at $0.9 < \alpha_c < 0.11$. Note the similarity with figure 2.

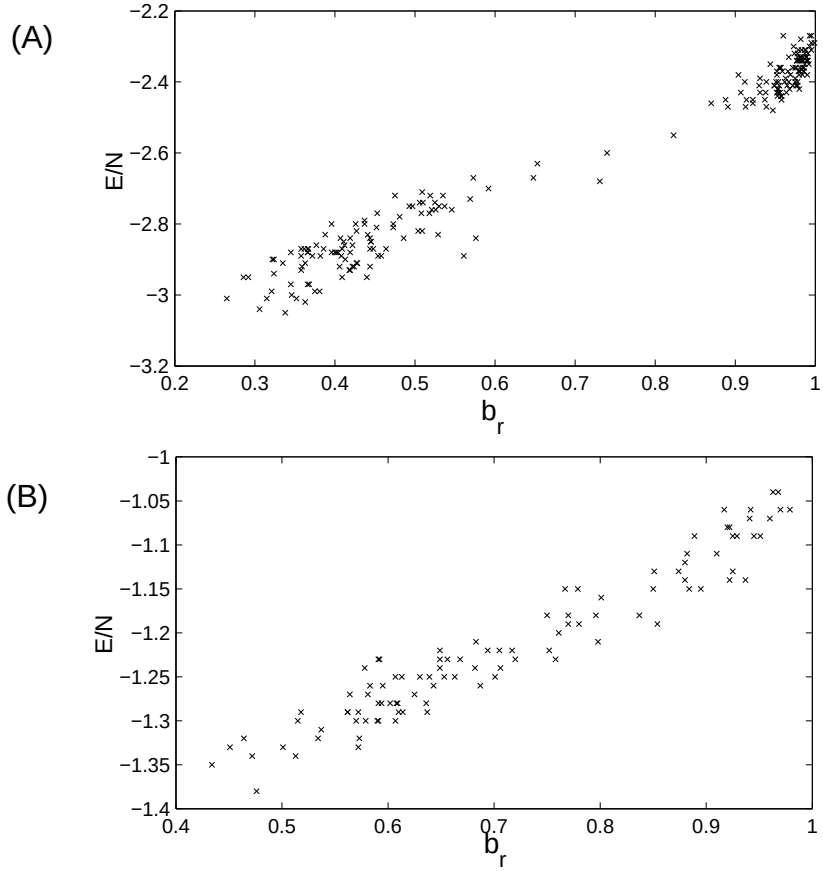


FIG. 4: Scatter plots of final energies and remanent overlaps for trajectories starting from memory patterns, for BGN above critical loading. (A) BGN with $N = 2000$, $\gamma = 2$ and $\alpha = p/N = 0.11$. Note that the overlap is strongly correlated with the energy and there is a gap in energy between the high and low-b_r states. This gap represents the latent heat of the phase transition. (B) BGN with $N = 2000$, $\gamma = 1$ and $\alpha = 0.2$. As in the $\gamma = 2$ case, the energy is strongly correlated with b_r, but the high and low groups overlap and the energy difference is smaller.

series of histograms at increasing N, one below the suspected transition and one above. As in the HN case, the transition grows sharper with increasing network size. Below the critical loading, the high-b peak remains robust as N increases, while above the critical loading the high-b peak shrinks with increasing network size and the low-b peak grows. Two quantitative differences are that the critical loading α_c is lower in the BGN case, $\alpha_c \approx 0.1$, while the average remanent overlap above the critical loading is higher, near 0.45.

The first-order nature of the transition is confirmed by examining the energies of the final states. These energies and the overlaps are shown in a scatter plot in figure 4A. The spin glass states associated with the low-b_r peak are clustered at energies below those of the retrieval states. The gap in energy between these two clusters corresponds to the latent heat of the phase transition.

B. BGN at low γ

For $\gamma = 0.5$, in contrast to $\gamma = 2$, the BGN's behaviour differs markedly from that of the HN. A series of $P(b_r)$ histograms for different values of p/N is shown in figure 5. Two features are evident. First, the stored patterns remain stable with few errors even up to high levels of storage, $\alpha = 0.3$. Second, there is no evidence of a discontinuous memory failure; rather, the retrieval quality as measured by b_r appears to degrade continuously as α increases. No second peak appears in the histograms; instead, the high-b peak first spreads and then begins to drift downward as errors accumulate.

At an intermediate value $\gamma = 1$ the $P(b_r)$ histograms (figure 6) suggest a first-order transition, although the evidence is less pronounced than in the $\gamma = 2$ case. A second peak appears above the transition, and the high-b_r

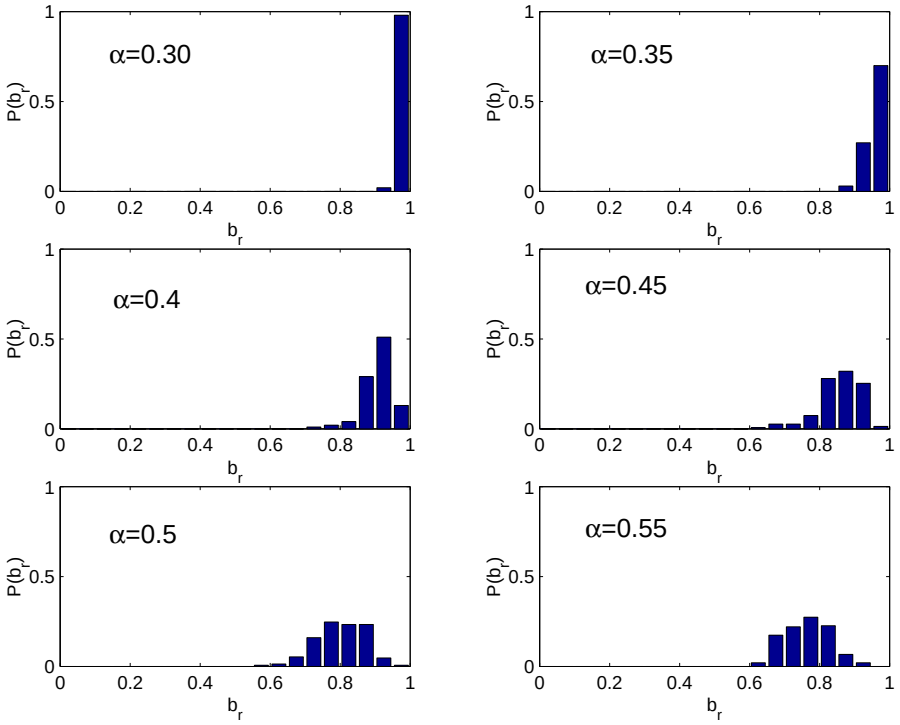


FIG. 5: Remanent bit overlap histograms for the BGN with $N = 1000$ and $\gamma = 0.5$, at a series of increasing values of the loading factor α. Few errors occur even at $\alpha = 0.3$, and the memory degrades gradually rather than abruptly with increasing α.

peak shows clear signs of shrinking as N increases, but the tails of the two peaks overlap substantially . The greater overlap between the peaks comes about for two reasons. First, the high-b_r peak above the critical loading is broader than in the $\gamma = 2$ case. Second, the remanent magnetisation is much higher (i.e., the drop in b_r at the critical point is much smaller.) The latent heat is also much smaller, as can be seen from the scatter plot of the energy (figure 4B). The critical loading, or storage capacity, is approximately 0.17, higher than for $\gamma = 2$ and higher than for the HN.

IV. ATTRACTORS, BASINS AND THE ENERGY LANDSCAPE AT HIGH LOADING

In the previous section, we examined the trajectories of initial conditions corresponding to memorized patterns and determined whether these trajectories remain close to the pattern or move away from it. Such experiments, however, probe only one aspect of network performance. We are interested not only in the stability of memory states but also in the sizes of their basins of attraction. The function of associative memory depends on the ability of the dynamics to correct partially corrupted patterns. More generally, we are interested in the evolution of the energy landscape with increasing α. To address these issues, we performed two additional sets of numerical experiments. First, we examined the attractors reached from a large number of *random* initial conditions to obtain a uniform sampling of the phase space and a broad picture of the energy landscape. Second, we examined the fate of initial conditions at specified Hamming distances from memory patterns. The latter set of experiments probes the landscape in the vicinity of the memory states. Results of similar experiments were given in ref. [2] for the case of low loading.

A. Evolution of the energy landscape: attractors reached from random initial states

In the case of the HN, it is known that in the thermodynamic limit the memory states are the lowest energy states for $\alpha < 0.05$, while for higher values of α spin glass states arise which have lower energies. Up to $\alpha_c \approx 0.148$ the memory states remain local minima of the energy even though they are not the global minima. Above α_c they cease

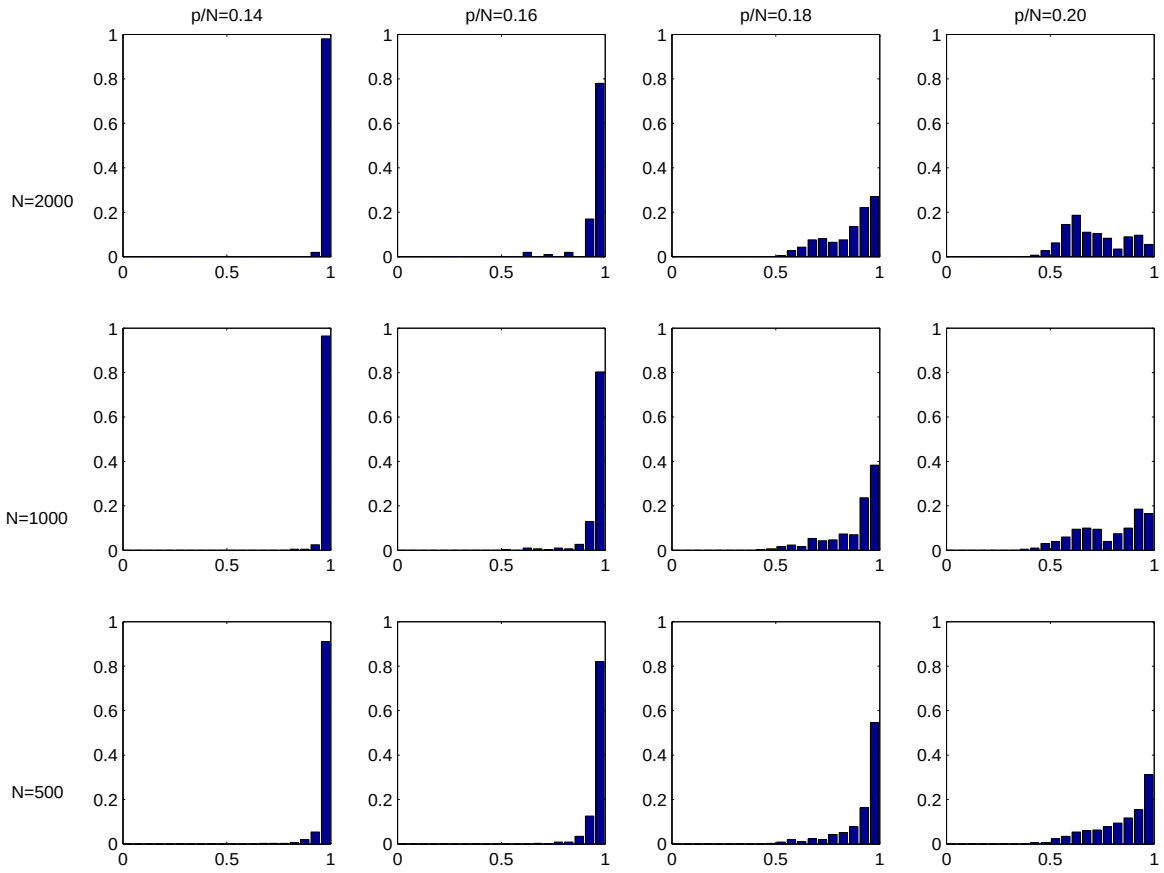


FIG. 6: Remanent overlap histograms for BGN with $\gamma = 1$ are consistent with a first-order transition at $0.16 < \alpha_c < 0.18$.

even to be local minima and therefore become unstable[9].[1] The drop in energy from the memory states to the spin glass states at α_c is the latent heat. One way to observe the evolution of the energy landscape is to examine the attractors reached from an ensemble of random initial conditions which effectively samples the configuration space. Figures 7-9 show histograms for the energies of attractors sampled in this manner. In each case, we sampled a total of at least 200 random initial conditions with several realizations of the random patterns $\boldsymbol{\xi}^\mu$. In figure 7, for the HN, we can see that at low loading the attractors are separated into two groups, the retrieval states at $E/N = -0.5$ and spurious states at a range of higher energies. The probability of retrieving a memory state from a random initial condition is high. With increasing α, the spurious states move to lower in energies until they are below the memory states. At the same time, their basins of attraction take up a larger portion of the configuration space, as is apparent from the growing size of the spin glass peak in the histogram and the shrinking size of the retrieval state peak. Figure 8 shows that for the BGN with $\gamma = 2$ the evolution is qualitatively similar. In figure 9, for $\gamma = 0.75$, we observe that an additional effect of high loading is to destabilize the uncondensed states. At low loading, the uncondensed states dominate the configuration space—almost all random initial conditions land on an uncondensed state, as was noted in [2]. The other two types of state begin to show their presence as the loading is increased, while the uncondensed states eventually disappear.

B. Retrieval of patterns from corrupted versions

To obtain information about the landscape in the vicinity of the memory states and about the shapes of their basins of attraction, we examined the fates of initial conditions which were not random but rather at specified initial overlaps

[1] For a schematic illustration of the evolution of the energy landscape, see fig. 2.18 of reference [7].

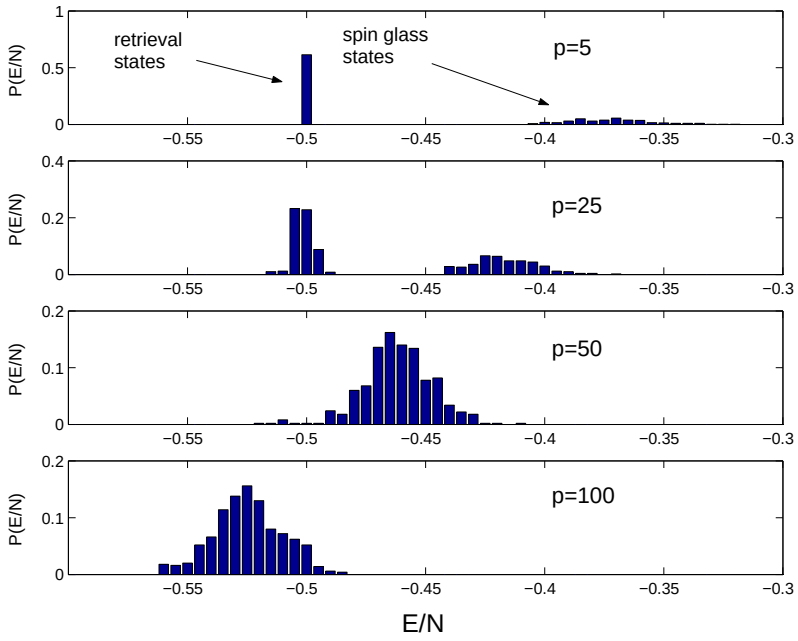


FIG. 7: Energy histograms of $P(E/N)$ for attractors reached from random initial states of the HN with $N = 1000$ nodes. As the number p of stored patterns increases, the peak at $E/N = -0.5$ corresponding to the retrieval states shrinks (and also spreads slightly) while the the spin glass states drift downward in energy until they are lower than the retrieval state energies.

with particular stored patterns. As in [2], these initial configurations were generated by starting with a particular "target" pattern and flipping the signs of a specified number of randomly chosen nodes. For each value of the initial overlap b_{init}, we generated an ensemble of initial conditions for several different realizations of the random set of memory patterns. We then evolved these states until the dynamics converged, and evaluated b_{final}, the final overlap with the target pattern, for each trajectory. If $b_{final} = 1$, this signifies that all signs which were initially flipped have been corrected and the target pattern has been retrieved perfectly. If $b_{init} < b_{final} < 1$, then the pattern has been retrieved imperfectly. The final state is closer to the stored pattern, but not all errors have been corrected. If $b_{init} > b_{final}$, then the trajectory has moved farther away from the stored pattern. As discussed in section II, the ability of the network to correct sign errors depends on the competition among the signal, the crosstalk, and the local potential. The initial states currently discussed have at least a moderately large overlap with the target pattern, resulting in a signal, and random overlaps with the other memory patterns, resulting in crosstalk.

Consider now the HN. At low loading, there is very little crosstalk. The crosstalk term is typically of order $\sqrt{p/N}$. If the HN is set in an initial condition whose overlap with the target pattern $\boldsymbol{\xi}$ is $b_{init} > \sqrt{p/N}$, then most nodes experience a net field which is aligned with the target pattern. Nodes which are initially misaligned with the target state ($x_i = -\xi_i$) will tend to change their signs and align with ξ_i. Each node which realigns in this way increases the value of b and thus increases the strength of the signal acting on the remaining nodes. As a result, even if in the initial state some fraction of the nodes experience a net field opposed to ξ_i, eventually the growing signal may overcome the crosstalk and correct those nodes as well. Therefore for low loading, as long as the initial state has $b_{init} > \sqrt{p/N}$, the probably of completely retrieving the target pattern is close to unity. As the loading ratio α increases, however, the typical crosstalk becomes stronger, and a higher signal is required to overcome the crosstalk noise. Therefore sign errors are not likely to be corrected unless the initial overlap is above a threshold, which grows higher with increasing α. If the crosstalk is too large, then some signs which are initially aligned with the pattern may be flipped, and the state may move away from the target pattern instead of toward it. Each node which flips out of alignment with the target pattern reduces the size of the overlap and hence of the signal, which makes other nodes more susceptible to crosstalk-induced errors, and a cascade of errors can occur. The critical loading α_c is the level at which even a state with $b_{init} = 1$ becomes unstable against such a cascade of errors.

Figure 10A shows a scatter plot of b_{final} vs. b_{init} for a HN slightly below critical loading. There is a threshold overlap for retrieval. If $b_{init} > 0.5$ the signal is strong enough to correct errors and the majority of trajectories flow towards the target pattern. For $b_{init} < 0.5$ the majority of trajectories move instead away from the target pattern. As α increases, the threshold value of b_{init} for retrieval increases until at α_c it reaches 1. The plot in figure 10A is

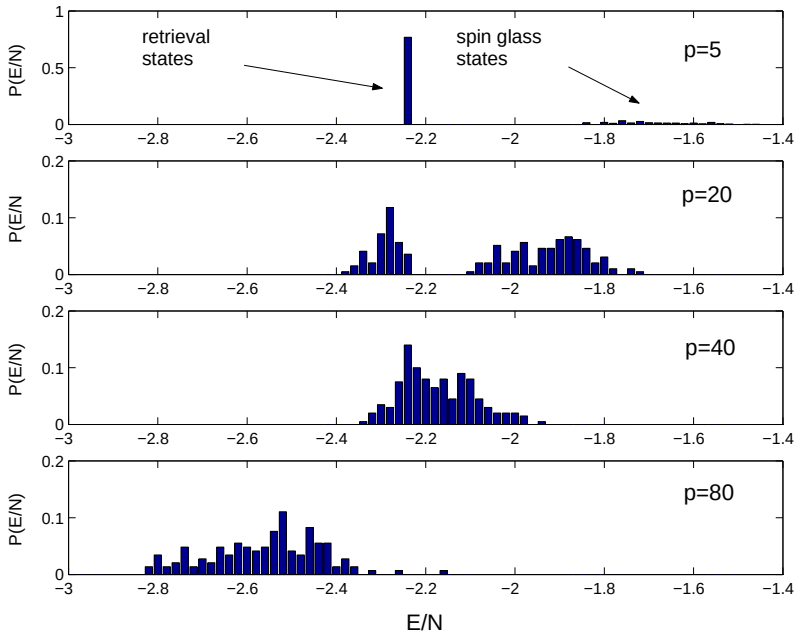


FIG. 8: Attractor energies from random initial conditions for BGN with $\gamma = 2$. Qualitative behaviour resembles that of the HN as shown in figure 7. One difference is that the spreading of the retrieval state energies with increasing loading is more pronounced.

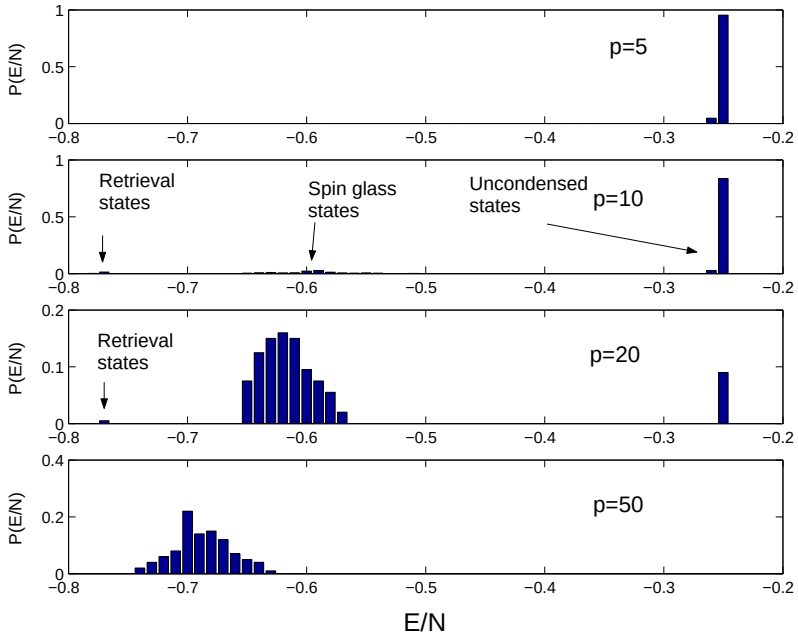


FIG. 9: Attractor energies from random initial conditions for BGN with $N = 1000$ and $\gamma = 0.75$. For low loading, the uncondensed states (with energy $E/N \approx -0.25$) fill most of the configuration space. The other two peaks in the histogram are very small. As the loading increases, however, the uncondensed states disappear. As in all cases, the "spin glass" peak grows larger with increasing α and shifts downward in energy.

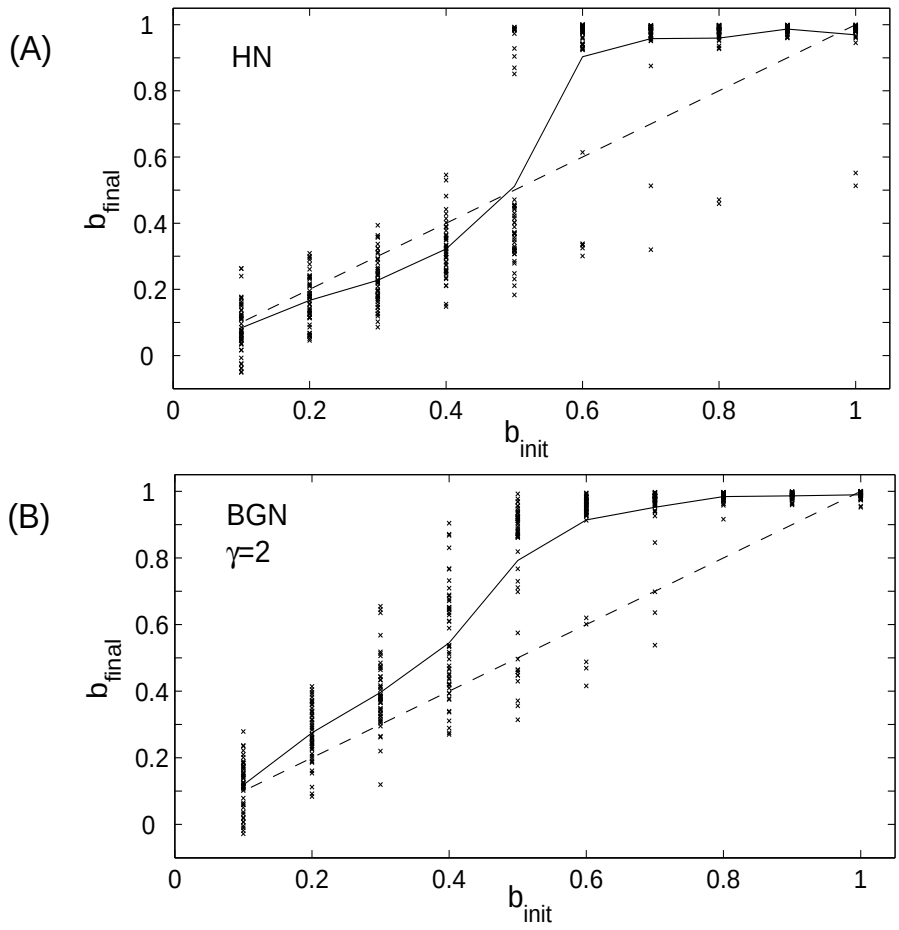


FIG. 10: Scatter plots of b_{final} vs. b_{init} for networks slightly below critical loading. Points show b_{final} for an ensemble of initial conditions with specified b_{init}. The average of b_{final} is shown by the solid curve. The dotted diagonal line $b_{final} = b_{init}$ is drawn for comparison: points above the line have $b_{final} > b_{init}$. (A) HN with $N = 2000$, $p = 260$. (B) BGN with $N = 2000$, $\gamma = 2$ and $p = 170$. In both cases, the retrieval quality as measured by b_{final} drops sharply for $b_{init} < 0.6$. For the BGN, however, the average b_{final} is always greater than b_{init}.

for a network with $N = 2000$; experiments with networks of different sizes reveal that the retrieval threshold becomes sharper as N increases.

In the BGN, on the other hand, the dynamics of error correction is more complicated due to the local potential. At strong coupling $\gamma \gtrsim 1$, the potential barriers against sign flips are less important than at weak coupling. As a result the BGN in this regime behaves in many respects like the HN. It is not surprising, then, that the scatter plot of b_{final} vs. b_{init} for a BGN with $\gamma = 2$ slightly below its critical loading (figure 10B) appears qualitatively similar to the corresponding figure 10A for the HN. There is a threshold (approximately $b_{init} = 0.6$) below which the probability of fully retrieving the target pattern drops sharply. Above this threshold, the signal is evidently strong enough to correct most sign errors. A key difference, however, is that even below this threshold the average b_{final} is larger than b_{init}. This means that the majority of a trajectories move toward the target pattern rather than away from it, but only some of the sign errors are corrected, not all.

In the case of the BGN with $\gamma = 0.5$, the local potential barriers are important, and interesting dynamics results from the competition among the signal from the target pattern, the crosstalk from other patterns, and the local potential. In the $\alpha \ll 1$ case [2], sign errors can be corrected only if the signal is strong enough to overcome the local potential barriers, and therefore there is a threshold value of the initial overlap which is much larger than $\sqrt{p/N}$. For the case $N = 1000$, $p = 5$, for example, we find that this threshold is approximately $b_{init} = 0.5$. For $b_{init} > 0.5$ there is a large probability that the target pattern is retrieved perfectly, while for $b_{init} < 0.5$ there is a large probability that the network will be stuck in an uncondensed state with $b_{final} = b_{init}$. In the intermediate range $0.4 < b_{init} < 0.6$, there is also a significant probability that the trajectory is attracted to an asymmetric spurious

state in which b_{final} is large but not unity and there are larger than random overlaps with one or more other memory patterns. This behaviour is illustrated by the scatter plot of figure 11A. As the loading increases (Figure 11A-D), something surprising happens: at first, the basins of attraction of the memory states *expand* slightly, contrary to what one would expect from the HN. The frontier of the uncondensed states is pushed back to lower values of b_{init}. For $p = 50$, or $\alpha = 0.05$ (fig. 11D) almost all states with $b_{init} > 0.1$ undergo some motion toward the target pattern, even if the pattern is not retrieved perfectly. As p increases further, the b_{final} vs. b_{init} plot preserves the approximate shape of fig. 11D.

The dynamics of retrieval and error correction for the BGN with weak coupling and high loading is evidently quite different from that of the HN. In the $\alpha = 0.05$ case of figure 11D, b_{final} is always 1 if $b_{int} = 1$, which means that the memory state is stable. However, it is retrieved only imperfectly when sign errors are introduced: if $b_{init} < 1$ then $b_{init} < b_{final} < 1$. This indicates that some nodes remain bistable and cannot be corrected. If the initial state is close to the target pattern, then the majority of errors are corrected, but that fraction decreases with decreasing b_{init}. Such a partial correction of errors does not often occur in the HN case. In the latter case, an initial condition either flows all the way to the retrieval state or moves away from it toward another attractor. The retrieval state may itself have a small number of errors due to crosstalk, but the presence of these errors does not depend on the initial state. The energy landscape of the HN in the neighborhood of a memory state apparently has the shape of a smooth basin — once the basin is entered, the trajectory usually runs without obstruction to the attractor at the bottom. For the weakly coupled BGN, on the other hand, the landscape appears to have the structure of a "funnel," [16][17][18] i.e., a sequence of local minima at decreasing energies, with low potential barriers separating each state from the next. There is a region of configuration space which has an overall tilt toward the retrieval state, but in which there are many local minima which may trap the trajectory before it reaches the retrieval state. This is illustrated schematically in figure 12. Funnel-shaped energy landscapes were first suggested in the context of protein folding dynamics.

V. A COMMENT ON SMALL NETWORKS

So far, this paper and the companion paper [2] have focused mainly on large networks of $N = 1000$ or more. However, some applications of neural network algorithms to robotics and other areas make use of networks of only 20 or 100 nodes. Experimental studies of BGN-like chemical reactor networks [14][15] used fewer than 10 nodes. The current work on the BGN was inspired in part by results suggesting that the BGN could store many more patterns than the HN, with fewer spurious attractors [12]. The latter results were inferred from a few selected cases using very small networks, and so we attempted to test the genericness of these results for a variety of small networks as well as for larger networks.

It should be noted that with very small networks, there are great fluctuations in properties depending on the particular set of memory patterns chosen, as it is impossible to ignore the mutual correlations among patterns. Results for the maximum storage capacity of a network are well-defined only in the thermodynamic limit $N \to \infty$, and for small N even an HN may in particular cases be able to store more than $0.14N$ stable patterns. For these reasons one cannot draw strong general conclusions about storage capacity based on small networks alone, but it is nonetheless instructive to make some comparative studies of pattern stability in small networks. For several small values of N and p, we generated random sets of stored patterns and tested their stability, using the HN and the BGN at several different values of γ. We counted the average fraction of memory patterns which were stable, f_{stable}.[2] In addition, we estimated the fraction of configuration space V_{spur} occupied by spurious attractors by following the trajectories of random initial conditions inside the hypercube $|x_i| < 2$. These results are collected in table I. In all cases the results were averaged over at least 100 sets of randomly generated patterns. In generating random sets of patterns, we did not eliminate cases in which two or more patterns are identical. The results show that, contrary to the selected examples discussed in [1] and [12], the spurious attractors do *not* generically occupy much less configuration space in the BGN than in the HN (in fact they normally occupy more, especially at low values of γ). However, for the most part the percentage of memory patterns which are stable is larger in the BGN than in the HN as long as $\gamma \lesssim 1$. As with larger networks, the BGN becomes most similar to the HN when $\gamma > 1$, while lower γ leads to increased pattern stability. The increased pattern stability at low γ is associated, however, with smaller basins of attraction for the memory states and therefore with a greater volume of phase space occupied by spurious

[2] In the thermodynamic limit there is an approximate permutation symmetry among the memory patterns, so that in general either all will be stable or none will be. By contrast, in small networks it is not unusual for some memorized patterns to reamain stable while others are not.

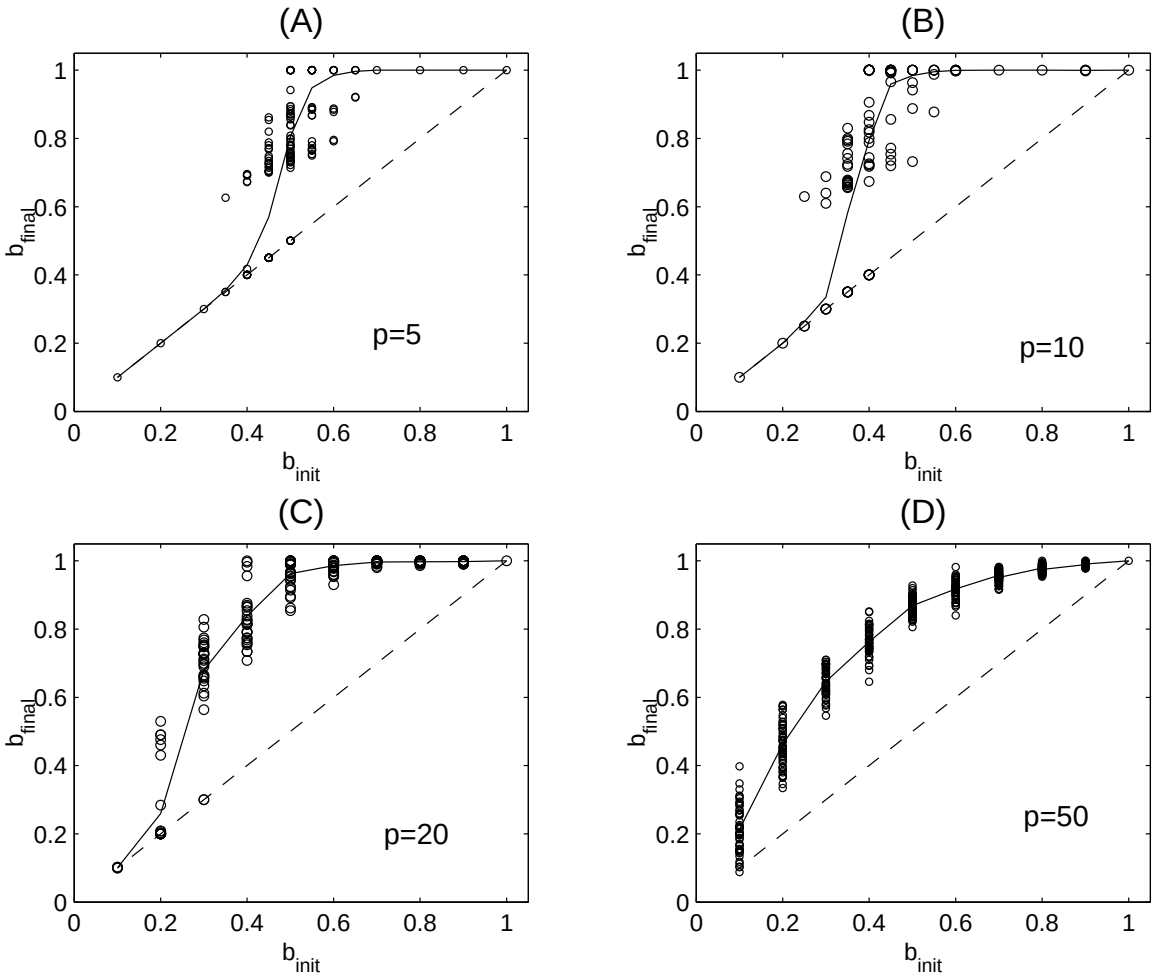


FIG. 11: Scatter plots showing pattern retrieval by the BGN with $N = 1000$, $\gamma = 0.5$. As in figure 10, the solid curve shows the average value of b_{final}. Uncondensed states lie on the line $b_{final} = b_{init}$: no sign flips occur and b maintains exactly its initial value. (A) $p = 5$ (B) $p = 10$ (C) $p = 20$ (D) $p = 50$.

states.

VI. DISCUSSION

We have studied the properties of the BGN at high memory loading α. Our results can be summarized as follows: For high values of γ, such as 2, there is a first-order transition similar to that of a HN. For $\gamma = 2$, the transition occurs at a critical loading $\alpha_c \approx 0.1$, which is lower than the critical loading of $\alpha \approx 0.148$ for the HN. As γ decreases, the critical loading increases and the phase transition evidently becomes weaker and eventually disappears. For $\gamma = 1$ the critical loading is apparently $\alpha_c \approx 0.17$ (higher than for the HN) and the phase transition is much less pronounced for the finite-size networks we have studied. For $\gamma = 0.5$ there is no evidence of a phase transition at all and patterns are stable with very few errors up to $\alpha \approx 0.3$.

A phenomenon that occurs in the BGN much more than in the HN is the partial retrieval of a pattern, whereby the dynamics corrects some sign errors in a pattern without correcting all of them. This is especially noticeable in the case of low γ and high α. This phenomenon suggests that in this case the energy landscape in the vicinity of a stored pattern has the shape of a funnel rather than a smooth basin of attraction. By a smooth basin of attraction, we mean a connected neighborhood which is sloped toward an attractor and in which there are few local minima that might obstruct a trajectory once it has begun to flow toward the attractor. By a funnel we mean a region with an

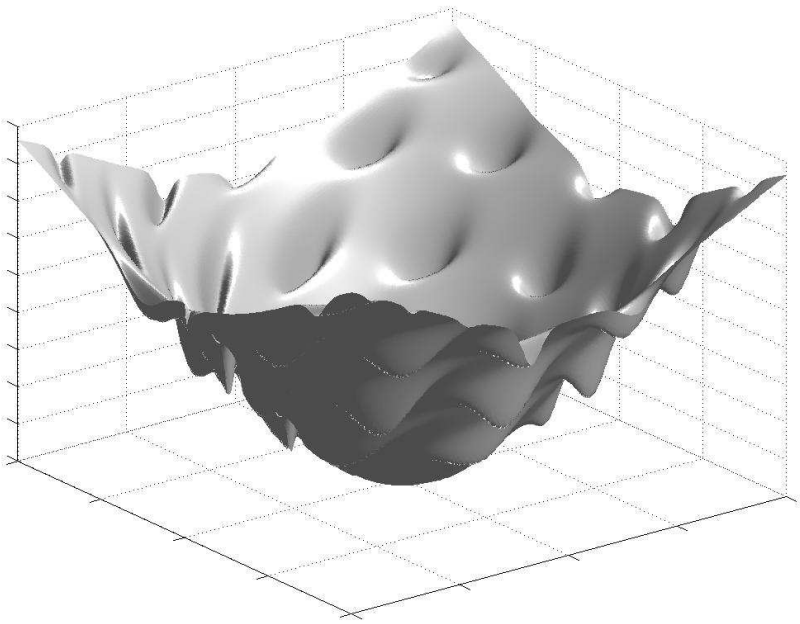


FIG. 12: Schematic picture of a funnel, or bumpy basin. Most trajectories travel some distance toward the global minimum (representing for example a memory state) but become trapped in a local minimum (a state with some errors) before reaching the bottom.

overall average slope toward an attractor which however contains many other local minima in which the trajectory might become stuck before reaching the bottom. The presence of these local minima is due to the bistability of the individual nodes and the local potential barriers against spin flips. These same potential barriers are also responsible for stabilizing the patterns. They make it less likely that crosstalk noise will induce an error in a pattern, but they also can inhibit the correction of an error which is present initially. Funnel-shaped landscapes were first examined in the context of protein folding dynamics[16][17]. It was suggested that at a finite temperature such a landscape would allow the protein dynamics efficiently to find the global minimum of energy in spite of the presence of numerous local minima separated by potential barriers. If indeed the landscape of the BGN at low γ forms a funnel, then it is possible that the introduction of some stochastic noise (i.e., finite temperature) could improve pattern retrieval by allowing trajectories to jump over the comparatively small potential barriers into lower energy minima, just as in the protein case. The effect of stochastic noise could be a fruitful subject for further study. An interesting question is whether there is an optimum level of noise which would improve the pattern retrieval ability of the BGN with low γ while at the same time maintaining the larger storage capacity. Intriguing questions remain concerning the dynamics of the BGN at low γ. The apparent initial expansion of the basins of attraction of the memory states with increasing loading is counterintuitive, and the patterns visible in figure 11 hint at some dynamics which is not yet fully understood.

Acknowledgments

This work was supported by Materials and Manufacturing Ontario (MMO), a provincial centre of excellence. Discussions with V. Chinarov are also acknowledged.

---

[1] V. Chinarov and M. Menzinger, Biosystems **55**, 137 (2000).

	$N=5, p=5$		$N=10, p=5$		$N=10, p=10$		$N=15, p=10$	
α	$V_{spur.}$	f_{stable}	V_{spur}	f_{stable}	V_{spur}	f_{stable}	$V_{spur.}$	f_{stable}
0.25	.38	.87	.96	1.00	.85	.92	.97	.97
0.5	.10	.68	.64	.91	.61	.51	.86	.65
0.75	.06	.49	.51	.75	.56	.32	.83	.37
1.0	.05	.37	.49	.62	.53	.23	.82	.23
1.5	.08	.37	.51	.47	.53	.16	.80	.15
2	06	.34	.43	.40	.51	.15	.85	.11
(HN)	.03	.34	.38	.48	.50	.16	.75	.15
	$N=20, p=5$		$N=20, p=10$		$N=50, p=5$		$N=100, p=5$	
α	V_{spur}	f_{stable}	$V_{spur.}$	f_{stable}	V_{spur}	f_{stable}	V_{spur}	f_{stable}
0.25	1.00	1.00	1.00	.99	1.00	1.00	1.00	1.00
0.5	.92	.99	.95	.74	.99	1.00	1.00	1.00
0.75	.78	.93	.92	.44	.78	1.00	.84	1.00
1.0	.71	.86	.92	.26	.61	1.00	.55	1.00
1.5	.71	.71	.91	.16	.57	.98	.46	1.00
2	.74	.62	.93	.11	.57	.97	.46	1.00
(HN)	.47	.78	.91	.20	.34	1.00	.34	1.00

TABLE I: Properties of small networks

[2] P. McGraw and M. Menzinger, preprint cond-mat/0203568, submitted to Phys. Rev. E.
[3] J.J. Hopfield, Proc. Natl. Acad. Sci. USA **79**, 2554 (1982).
[4] W.A. Little, Math. Biosci. **19**, 101 (1974). W.A. Little and G.L. Shaw, Math. Biosci. **39**, 281 (1978).
[5] S. Haykin, Neural Networks: A Comprehensive Foundation. Prentice Hall, Upper Saddle River, NJ, 1999.
[6] Daniel J. Amit, Modeling Brain Function: The World Of Attractor Neural Networks. Cambridge University Press 1989.
[7] J. Hertz, A. Krogh and R.G. Palmer, Introduction to the Theory of Neural Computation. Perseus Books, Cambridge, MA 1991.
[8] D.J. Amit, H. Gutfreund and H. Sompolinsky, Phys.Rev. **A32**, 416 (1985); Phys. Rev. Lett. **55**, 428 (1985);
[9] D.J. Amit, H. Gutfreund and H. Sompolinsky, Ann. Phys. **173**, 30 (1987). A. Chrisanti, D.J. Amit and H. Gutfreund, Europhys. Lett. **2**, 337 (1986).
[10] D.O. Hebb, The Organization of Behavior, Wiley, New York, 1949.
[11] J.J. Hopfield, Proc. Natl. Acad. Sci. USA **81**, 3088 (1984).
[12] V. Chinarov and M. Menzinger, "Bistable Gradient Networks: Their Computational Properties" in J. Mira and A. Prieto, eds., Connectionist Models of Neurons, Learning Processes, and Artificial Intelligence, p.333. Springer Verlag, Berlin 2001.
[13] M. Mezard, G. Parisi and M. Virasoro, Spin Glass Theory and Beyond. World Scientific, Singapore, 1987.
[14] W. Hohmann, M. Krauss and F.W. Schneider, J. Phys. Chem. A **103**, 7606 (1999); J Phys. Chem A 102, 3103 (1998); J. Phys. Chem A 101, 7364 (1997). G. Dechert, K.-P. Zeyer, D. Lebender and F.W. Schneider, J. Phys Chem A 100, 19043 (1996).
[15] J.-P. Laplante, M. Pemberton, A. Hjelmfelt and J. Ross, J. Phys. Chem 99, 10063 (1995). V. Booth, T. Erneux and J.-P. Laplante, J. Phys. Chem 98, 6537 (1994). A. Hjelmfelt and J. Ross, J. Phys. Chem. 97, 7998 (1993).
[16] P.E. Leopold, M. Montal and J.N. Onuchic, Proc. Natl. Acad. Sci. USA **89**, 8721 (1992).
[17] P. Wolynes et al. Science **267**, 1618 (1995).
[18] O.M. Becker and M. Karplus, J. Chem Phys. **106**, 1495 (1997).